Chemosphere 280 (2021) 130687

Contents lists available at ScienceDirect

Chemosphere

journal homepage: www.elsevier.com/locate/chemosphere

Mathematical modeling and numerical simulation of sulfamethoxazole adsorption onto sugarcane bagasse in a fixed-bed column

Diego Juela [a], Mayra Vera [b], Christian Cruzat [b], Ximena Alvarez [b], Eulalia Vanegas [b, *]

[a] Chemical Engineering, Faculty of Chemical Sciences, University of Cuenca, 010203, Cuenca, Ecuador
[b] Center for Environmental Studies, Department of Applied Chemistry and Production Systems, Faculty of Chemical Sciences, University of Cuenca, 010203, Cuenca, Ecuador

HIGHLIGHTS

- Adsorption of sulfamethoxazole with sugarcane bagasse was investigated.
- A new mechanistic model was developed and solved numerically.
- Eight analytical models were used to fit the breakthrough data.
- The mechanistic model predicted breakthrough curves with great accuracy.
- The Log-Gompertz model correlated well with asymmetric breakthrough curves.

GRAPHICAL ABSTRACT

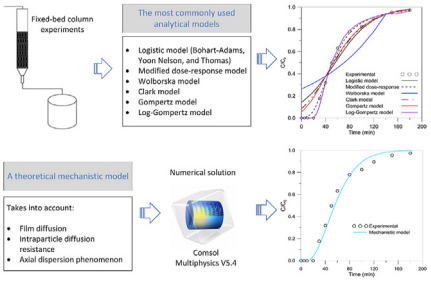

ARTICLE INFO

Article history:
Received 22 January 2021
Received in revised form
19 April 2021
Accepted 20 April 2021
Available online 27 April 2021

Handling Editor: Yongmei Li

Keywords:
Analytical models
Fixed-bed column
Dynamic simulation
Wastewater treatment
Biosorption
Breakthrough curve

ABSTRACT

Having rigorous mathematical models is essential for the design and scaling of adsorption columns. In this study, the dynamic behavior of the sulfamethoxazole adsorption on sugarcane bagasse was studied and compared using analytical models and a theoretical mechanistic model. Initially, fixed-bed column tests were carried out at different flow rates and bed heights. Then, the experimental data were fitted with the most widely used analytical kinetic models, and their fit and fixed-bed parameters were compared with the mechanistic model. Of all analytical models analyzed, the Log-Gompertz model was the one that had the best agreed with experimental data. Although some analytical models fitted the experimental data accurately, their usefulness was questionable. Their parameters did not show a clear relationship with the change in operating conditions, and in certain cases had different behavior from that observed in experimentation. Conversely, the mechanistic model not only predicted the breakthrough curves with great accuracy in the initial and transition stage ($R^2 > 0.92$; SSE < 0.06), but it also estimated relevant parameters. Additionally, the effects of the global mass transfer coefficient (K_i) and the axial dispersion coefficient (D_z) on breakthrough curves were studied using the mechanistic model. Increasing K_i increased the slope of the breakthrough curves with a faster adsorption rate. Similarly, high values of D_z produced lower adsorption capacities of the adsorbent; and it was established that the axial dispersion is relevant in SMX adsorption on SB. The theoretical model presented can be used for the design, scaling, and optimization of adsorption columns.

* Corresponding author. University of Cuenca, Av. 12 de Abril, 010203, Cuenca, Ecuador.
E-mail address: eulalia.vanegas@ucuenca.edu.ec (E. Vanegas).

https://doi.org/10.1016/j.chemosphere.2021.130687
0045-6535/

Nomenclature

Notation

a	parameter of the Logistic model
a'	model parameter of the modified dose-response model
b	parameter of the Logistic model
B	unidimensional parameter of the Clark model
C	SMX final concentration (mg/L)
C_e	SMX concentration in the liquid phase at equilibrium (mg/L)
C_0	SMX initial concentration (mg/L)
C_R	concentration of SMX adsorbed (mg/L)
d_p	average diameter of the adsorbent particle (m)
D	column diameter (m)
D_m	molecular diffusion coefficient (m^2/s)
D_{ep}	effective pore diffusivity coefficient (m^2/s)
D_p	pore diffusion coefficient (m^2/s)
D_s	surface diffusion coefficient (m^2/s)
D_z	axial dispersion coefficient (m^2/s)
H_b	fraction of the saturated bed (%)
m	mass of adsorbent (g)
M_s	molecular weight of the solvent (g/mol)
N_0	adsorption capacity of BCA per unit volume of the bed (mg/L)
K	distribution ratio equal to q_0/C_0
K_i	global mass transfer coefficient (1/s)
k_{BA}	Bohart-Adams' rate coefficient (L/mg min)
k_f	external film mass transfer coefficient (m/s)
k_L	energy constant related to the heat of adsorption (L/mg)
k_{Th}	Thomas rate coefficient (1/min)
k_{YN}	Yoon-Nelson rate coefficient (L/mg min)
Pe	Peclet number
q	SMX concentration in the solid phase at time t (mg/g)
q_e	adsorption capacity at saturation time or equilibrium (mg/g)
q_F	adsorption capacity predicted by the analytical model (mg/g)
q_0	adsorption capacity in equilibrium with C_0 from Batch studies (mg/g)
q_{max}	maximum adsorption capacity of the Langmuir isotherm (mg/g)
Q	flow rate of the solution (mL/min)
r	model parameter of the Clark model (1/min)
r_p	average radius of the adsorbent particle (m)
Re	Reynolds number
R_p	particle radius (m)
Sc	Schmidt number
T	temperature of the SMX solution (K)
t_b	breakthrough time (min)
t_s	saturation time (min)
v_i	interstitial velocity of the solution (m/s)
v_s	superficial velocity of the solution (m/s)
V_m	molar volume of SMX at its normal boiling point (cm^3/mol)
Z	bed height (m)
z	distance along the bed (m)

Greek Letters

α	velocity of constant pattern front
α_G	parameter of the Gompertz model
α_A	solvent association parameter
β	external mass transfer coefficient (1/min)
β_G	parameter of the Gompertz model (1/min)
ρ	density of the SMX solution (kg/m^3)
ρ_b	bed bulk density (kg/m^3)
ρ_p	density of the adsorbent particle (kg/m^3)
μ	dynamic viscosity of the solution (kg/cm.s)
ε_b	bed void fraction or bed porosity
ε_p	particle porosity
τ	time required for 50% breakthrough (min)
τ_p	tortuosity factor of the adsorbent

1. Introduction

Sulfamethoxazole (SMX) is a bacteriostatic antibiotic, and it is one of the most common sulfonamides consumed in human and veterinary medicine, especially in high-income countries (Klein et al., 2018). A conventional wastewater treatment plant (WWTP) is not designed to completely remove SMX residues present in wastewaters (Sun et al., 2016; Zhang et al., 2015). In WWTPs, SMX is partially removed by microbiological degradation and adsorption in sludge (da Silva Rodrigues et al., 2020; Ekpeghere et al., 2017). As a consequence of incomplete removal of SMX, this antibiotic is one of the most commonly detected in wastewaters, groundwaters, surface and drinking waters in concentrations ranged from ng/L to μg/L (Wang and Wang, 2018; Wilkinson et al., 2017). The concern regarding SMX in aquatic environments is due to this antibiotic has the ability to accumulate in aquatic organisms. SMX has a bioconcentration factor of 2.80, which is much higher than other antibiotics (Liu et al., 2018b); SMX also has a hazard ratio of 34.81 (Liu et al., 2018a), which allows its accumulation in fish, shrimp, and other aquatic organisms. This makes it a high-risk antibiotic for the aquatic environment as well as for the food chain. Besides, many studies have reported some toxicity effects of SMX on aquatic organisms. For instance, in microalgae, it has been shown that SMX destroys cell wall synthesis and disrupts photosynthesis pathways (Välitalo et al., 2017); it leads to a general decrease in the utilization of the carbon source in the periphyton (Johansson et al., 2014). In bioluminescent bacteria such as *Vibrio fischeri*, SMX affects their enzymatic system and therefore reduces their bioluminescence by 50% (Prasannamedha and Kumar, 2020). All of these effects occur when aquatic organisms are exposed to concentrations in the mg/L range, so SMX levels found in surface and drinking waters are not high enough to affect human and animal health. However, due to the frequent, extensive, and uninterrupted use of these types of drugs, these very low concentrations can pose a threat to the development of antibiotic-resistant bacteria.

Adsorption is a low-cost and efficient technology that can be used to remove SMX and other antibiotics from wastewaters. Materials like activated carbon (Serna-Carrizales et al., 2020), biochar (Zeng et al., 2021), carbon nanotubes (Chen et al., 2017), graphene and its derivates (Masri et al., 2020), metal-organic frameworks (Yu et al., 2020), clays and minerals (Wu et al., 2019), and agricultural residues (Peñafiel et al., 2020) has been used as adsorbents for SMX adsorption. In agro-industrial countries like Ecuador, where a large number of residues is produced annually, natural adsorbents are more attractive. Sugarcane bagasse (SB) is one of these residues that has shown high potential to remove pollutants from

wastewaters (Ahmad et al., 2018; Juela, 2020; Nardy Ribeiro et al., 2011; Vera et al., 2018). Adsorption can be carried out in a batch process or in fixed-bed columns. However, the latter has greater advantages due to its simple mode of operation, suitable for large volumes, easy to scale up from laboratory to pilot or industrial operation, and it is applicable to the operation mode of WWTPs (Ahmed and Hameed, 2018). In order to design efficient adsorption columns, it is necessary to understand the main mechanisms involved in the adsorption of a given adsorbate-adsorbent system. Many mathematical models have been developed to elucidate these mechanisms and predict the breakthrough curve of a given adsorption system.

Analytical kinetic models such as the Yoon-Nelson, Thomas, Bohart-Adams, Modified dose-response, and Bed Depth Service Time model have been used to estimated kinetic parameters for continuous adsorption of SMX (Jaria et al., 2019; Li et al., 2020; Tian et al., 2013; Zeng et al., 2021). The Thomas model correlated well with experimental data on the SMX adsorption with lignite activated carbon, and this revealed that the SMX adsorption could be dominated by film diffusion (Li et al., 2020). Similarly, Jaria et al. (2019) used the Thomas, Yoon-Nelson, and Modified dose-response models to analyze the dynamic behavior of the SMX adsorption into granular activated carbon, and the modified dose-response model was the one that best fit the experimental data in all tests. Although these models fit with some precision to a real adsorption process, these models are not based on a mechanistic approach and ignore intraparticle diffusion resistance and axial dispersion, and all of these models require experimental breakthrough curves to estimate their respective parameters (Unuabonah et al., 2019). Besides, several studies have questioned the practical utility of classic analytical models due to their inaccuracy in predicted fixed-bed parameters (Dorado et al., 2014; Jaria et al., 2019; Li et al., 2020). For instance, Dorado et al. (2014) found that the adsorption capacity predicted by the modified-dose response model and Wolborska model were 100 times lower than those measured, or had an unexpected behavior with operating conditions. Due to these disadvantages of these models, in the last decades, several theoretical mathematical models have been developed to describe the dynamic behavior of a fixed-bed adsorption column. Most of these models are composed of a macroscopic mass conservation equation, a kinetic equation, and an equilibrium relationship or isotherm, which can be solved numerically using computational software. These theoretical models take into account both film and intraparticle diffusion, hence these are more closely approximate a real adsorption process with a higher degree of accuracy (Unuabonah et al., 2019). Additionally, a mechanistic model can estimate valuable parameters such as mass transfers and axial dispersion coefficients.

In this work, six most widely used analytical kinetic models (the Thomas, Yoon-Nelson, Bohart-Adams, Clark, Modified dose-response, Wolborska models) and two recently developed models (the Gompertz and Log-Gompertz models) were applied to fit the breakthrough experimental data under different operation conditions for the SMX adsorption into SB. Then, the best-fitted analytical model was compared with a theoretical mechanistic model, which considered film diffusion, intraparticle diffusion, and axial dispersion. The mechanistic model was also used to evaluate the effects of global mass transfer coefficient and axial dispersion coefficient on the breakthrough curves. Finally, the relative importance of the axial dispersion phenomenon was assessed by comparison with other rate mechanisms.

2. Theory

2.1. Analytical kinetic models of fixed-bed column adsorption

The biosorption process in continuous systems is a dynamic process since the adsorbate concentration varies with time, as well as throughout the column. This particular dynamic behavior of a column packed with a biosorbent is described by its breakdown curve. This curve can be obtained through experimentation or the application of mathematical models. In the available literature, there are many analytical models that have been used to predict the breakthrough curve in liquid phase. In this study, eigth models were used to study the performance and predict the fixed bed column parameters: Yoon-Nelson, Thomas, Bohart-Adams, Wolborska, Modified dose-response, Clark, Gompertz, and Log-Gompertz models. The Bohart-Adams, Yoon-Nelson, and Thomas models were unified as a single model called “Logistic model” due to they are mathematically equivalent according to various studies (Bakka et al., 2020; Chu, 2020a; Dima et al., 2020). After applying the Logistic model, the parameters of the Bohart-Adams, Yoon-Nelson, and Thomas models were estimated using simple correlations as shown in Fig. 1. The breakthrough and linear equations of all these models are shown in Table 1.

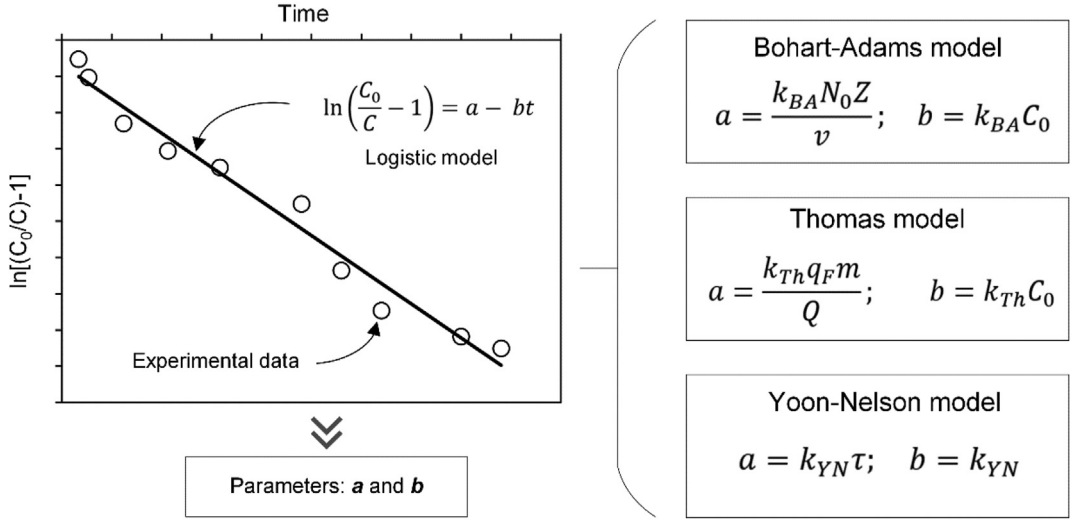

Fig. 1. Scheme to obtain the Bohart-Adams, Thomas, and Yoon-Nelson parameters using the Logistic model.

Table 1
Analytical kinetic models used in this study.

Model			Plot	Parameters	Reference
Logistic model	Non-Linear	$\frac{C}{C_0} = \frac{1}{1+\exp(a-bt)}$	$\ln\left(\frac{C_0}{C}-1\right)$ vs t	k_{BA} (L/mg min) and N_o (mg/L) for Bohart-Adams models; k_{Th} (L/mg min) and q_F (mg/g) for Thomas model; k_{YN} (1/min) and τ (min) for Yoon-Nelson model.	Chu (2020a)
	Linear	$\ln\left(\frac{C_0}{C}-1\right) = a - bt$			
Wolborska model	Non-Linear	$\frac{C}{C_0} = exp\left(\frac{\varepsilon_b \beta C_0}{\rho q_F} t - \frac{\beta Z}{u}\right)$	$\ln\left(\frac{C}{C_0}\right)$ vs t	β is the external mass transfer coefficient (1/min), and q_F is the adsorption capacity provided by the Wolborska model (mg/g).	Wolborska and Pustelnik (1996)
	Linear	$ln\left(\frac{C}{C_0}\right) = \frac{\varepsilon_b \beta C_0}{\rho q_F} t - \frac{\beta Z}{u}$			
Modified dose-response model	Non-Linear	$\frac{C}{C_0} = 1 - \frac{1}{1+\left(\frac{C_0 Qt}{q_F m}\right)^{a'}}$	$\ln\left(\frac{C}{C_0-C}\right)$ vs $\ln(C_0Qt)$	a' is the model parameter, and q_F is the adsorption capacity provided by the modified dose-response model (mg/g).	Yan et al. (2001)
	Linear	$\ln\left(\frac{C}{C_0-C}\right) = a' \ln(C_0 Qt) - a' \ln(q_F m)$			
Clark model	Non-Linear	$\frac{C}{C_0} = \left(\frac{1}{1+B^*\exp(-rt)}\right)^{\frac{1}{n-1}}$	$\ln[(C_0/C)^{1/n}-1]$ vs t	r is the model parameter (1/min), B is an unidimensional parameter of the Clark model, and n is a parameter of the Freundlich isotherm.	Xu et al. (2013)
	Linear	$ln\left[\left(\frac{C_0}{C}\right)^{n-1} - 1\right] = -rt + \ln(B)$			
Gompertz model	Non-Linear	$\frac{C}{C_0} = exp[-\exp(\alpha_G - \beta_G t)]$	$\ln\left[\ln\left(\frac{C_0}{C}\right)\right]$ vs t	α_G and β_G (1/min) are parameters of Gompertz model.	Chu (2020b)
	Linear	$ln\left[\ln\left(\frac{C_0}{C}\right)\right] = \alpha_G - \beta_G t$			
Log-Gompertz model	Non-Linear	$\frac{C}{C_0} = exp[-\exp(\alpha_G - \beta_G \ln t)]$	$\ln\left[\ln\left(\frac{C_0}{C}\right)\right]$ vs ln t	α_G and β_G (1/min) are parameters of Gompertz model.	Chu (2020b)
	Linear	$ln\left[\ln\left(\frac{C_0}{C}\right)\right] = \alpha_G - \beta_G \ln t$			

2.2. Approach to a theoretical mechanistic model

The analytical models named above were compared with a theoretical mechanistic model. This model was defined as a set of equations for the biosorbent bed layer, and it is based on the mass balance of SMX in the liquid phase, a kinetic model, and an equilibrium model.

The general mass balance equation for the transport and adsorption of diluted species in porous media when the pore space is primarily filled with liquid but also contains pockets or immobile gas is described as shown in Eq. (1).

$$\varepsilon_b \frac{\partial(C)}{\partial t} + \rho_b \frac{\partial(q)}{\partial t} - \nabla(D_z - D_e)\nabla C + \frac{\partial(v_s C)}{\partial z} = R \quad (1)$$

where, C (mg/L) and q (mg/g) are the SMX concentration in the liquid and solid phase, respectively, ε_b and ρ_b (kg/m^3) are the bed void fraction and bed bulk density, respectively. D_z (m^2/s) and D_e are (m^2/s) are the axial dispersion coefficient and volatilization coefficient, respectively, and v_s (m/s) is the superficial velocity. On the left side of Eq. (1), the first two terms correspond to the SMX concentration within the liquid and solid phase, the following term introduces the dispersion (D_z) and volatilization (D_e) phenomenon in the x, y, and z directions. While the last term describes mass transfer by convection. On the right-hand side, R describes the rate of the adsorption reaction. The volatilization and reaction adsorption were neglected ($D_e = 0$, $R = 0$) for being a little influential in aqueous phase adsorption (Xu et al., 2013). Besides, it was considered that there is an SMX concentration gradient only in the longitudinal direction (z-axis) of the column. The variation of superficial velocity along the longitudinal direction of the bed was estimated using Eq. (2) (Babu and Gupta, 2005).

$$\rho \frac{\partial(v_s)}{\partial z} = -(1-\varepsilon_b)\rho_b \frac{\partial q}{\partial t} \quad (2)$$

where ρ (kg/m^3) is the density of the SMX solution. The adsorption kinetic model used in this study was the Linear driving force (LDF) model. In this model, the intrapellet diffusion rate is represented by a lumped mass transfer coefficient and is shown in Eq. (3) (Naidu and Mathews, 2021).

$$\frac{\partial q}{\partial t} = K_i(q_e - q) \quad (3)$$

where, K_i (1/s) is the global mass transfer coefficient and q_e (mg/g) is the SMX concentration within the adsorbent particle at equilibrium. In Eq. (3), K_i combined both the film diffusion and intraparticle diffusion. Besides, within the intraparticle mass transfer, both surface diffusion and pore diffusion were considered, since both are simultaneously involved according to several studies (Kavand et al., 2018; Xu et al., 2013). Finally, the adsorption equilibrium model used was the Langmuir isotherm, Eq. (4), according to our previous batch studies carried out in our department (Zeas Solórzano and Zhunio Campoverde, 2019).

$$q_e = \frac{q_{max} k_L C_e}{1 + k_L C_e} \quad (4)$$

where, q_{max} (mg/g) is the maximum adsorption capacity, k_L (L/mg) is the energy constant related to the heat of adsorption, and C_e (mg/L) is the SMX concentration in the liquid phase at equilibrium. These equilibrium data were estimated at a temperature of 20 °C and are presented in Table 3.

2.2.1. Boundary and initial conditions

The boundary and initial conditions to solve Eqs. (1) and (3) are describing as follows (Danckwerts, 1953).

$$t = 0 \;:\; C = 0,\; q = 0 \quad (0 \le z \le Z) \quad (5)$$

$$z=0 \ : \ \frac{\partial C}{\partial z}=\frac{v_s}{D_z}(C-C_0) \ (t>0) \quad (6)$$

$$z=Z \ : \ \frac{\partial C}{\partial z}=0 \quad (t>0) \quad (7)$$

The velocity boundary conditions are given by the following equations.

$$z=0 \ : \ v_s=v_0 \quad (t>0) \quad (8)$$

$$z=Z \ : \ \frac{\partial v_s}{\partial t}=0 \quad (t>0) \quad (9)$$

where z (cm) is the longitudinal direction of the column, Z (cm) is the bed height, C_0 (mg/L) is the initial concentration of SMX at the top of the bed, and v_0 (m/s) is the velocity of the SMX solution at the top of the bed (Babu and Gupta, 2005).

2.2.2. Parameters' estimation

Several additional parameters are necessary to solve the mechanistic model. Empirical correlations were used to estimate the axial dispersion coefficient D_z, the global mass transfer coefficient K_i, the film diffusion coefficient k_f, the SMX molecular diffusion coefficient D_m, the effective pore diffusion coefficient D_{ep}, the pore diffusion coefficient D_p, surface diffusion coefficient D_s, the tortuosity factor τ_p, the Reynolds number Re, the Schmidt number Sc, and the Peclet number Pe. All these parameters were estimated using Eqs. (10)-(18) and are shown in Table 2.

Where, ε_p is the particle porosity, d_p (m) and r_p (m) are the average diameter and average radius of the adsorbent particle, α_A is a solvent association parameter, M_s (g/mol) is the molecular weight of the solvent, T (K) is the temperature of the SMX solution, V_m (cm^3/mol) is the molar volume of SMX at its normal boiling point, ρ (kg/m^3) and μ (kg/m.s) are the density and dynamic viscosity of the SMX solution, and v_s (m/s) is the superficial velocity through the bed. The properties of SB and SMX used to estimate the parameters are described in Table 3. The methodology used to measure equilibrium (Zeas Solórzano and Zhunio Campoverde, 2019), fixed-bed parameters (Vera et al., 2016), and sugarcane bagasse properties (Juela, 2020; Peñafiel et al., 2021) is detailed in our previous studies.

2.3. Numerical solution

The model was implemented and solved numerically in Comsol Multiphysics V5.4. The module of partial differential equations (PDE) was used in this study; three PDE modules were used to represent the Eqs. (1)–(3), according to the methodology described by Aguilera and Ortiz (2016). The time-dependent and one-dimensional model was solved using the finite element method.

3. Materials and methods

3.1. Adsorbent and adsorbate

Raw SB was obtained from a local sugar mill in Azuay, Ecuador. Before their use in adsorption tests, SB was washed repeatedly with distilled water in order to remove impurities and residual sugars. Then, sugarcane marrow was dried in an oven at 60 °C for 8 h. Finally, the size of the fibers was reduced using a hammer mill and subsequent. Particles between 0.841 and 0.42 mm were used in adsorption experiments.

SMX with a purity of 99.00% supplied by Sigma-Aldrich was used in this study. Methanol of analytical grade Merck with a purity of 99.00% was used to dissolve SMX. The SMX solutions were prepared with distilled water and with 1% V/V methanol. All synthetic solutions had a concentration of 5 mg/L of SMX. The pH of the solution was adjusted to 6 with the addition of HCl (0.1 N) solution.

3.2. Packed column tests

A glass column with a size of 35 cm height and 2.2 cm internal diameter was used for the adsorption tests. The system was operated with downward flow, and at a temperature of 18 °C. For the experimental setup of the column, initially, 1 cm of gravel of 2 mm diameter was placed at the bottom of the column to prevent the adsorbent from being entrained by the solution, then the adsorbent previously weighed was introduced into the inside the column, then 1 cm of gravel of 2 mm diameter was placed on the top of the fixed bed in order to avoid the floating of the bed and provide a better distribution to the SMX solution. A peristaltic pump was used to pump the SMX solution up to the column inlet. SMX samples were periodically collected at the column outlet. The initial and residual concentrations of SMX were determined by the Visible Genesys 10S UV spectrophotometry technique from Thermo SCIENTIFIC, at a wavelength of 261 nm. The experimental

Table 2
Empirical correlations used to estimate the fixed-bed column parameters.

Parameter	Unit	Empirical correlation		Reference
D_z	m^2/s	$\frac{v_i d_p}{D_z}=0.2+0.011\left(\frac{Re}{\varepsilon_b}\right)^{0.48}$	(10)	Soriano et al. (2016)
K_i	1/s	$\frac{1}{K_i}=\frac{r_P}{3k_f}\frac{\rho_p q_0}{C_0}+\frac{r_p^2}{15\varepsilon_p D_{ep}}\frac{\rho_p q_0}{C_0}$	(11)	Ruthven (1984)
k_f	m/s	$\frac{k_f d_p}{D_m}=2+1.58Re^{0.4}Sc^{1/3}$	(12)	Ohashi et al. (1981)
D_m	m^2/s	$D_m=7.4{*}10^{-8}\frac{(\alpha_A M_s)^{0.5}T}{\mu V_m^{0.6}}$	(13)	Wilke and Chang (1955)
D_{ep}	m^2/s	$D_{ep}=\frac{D_s+D_p}{f'(C)\rho_b}$	(14)	Xu et al. (2013)
D_p	m^2/s	$D_p=\frac{\varepsilon_p D_m}{\tau_p}$	(15)	Xu et al. (2013)
D_s	m^2/s	$\frac{15D_s}{r_p^2}=0.00129\left(\frac{D_m C_0}{r_p^2 q_0}\right)^{1/2}$	(16)	Xu et al. (2013)
τ_p	–	$\tau_p=\varepsilon_p+1.5(1-\varepsilon_p)$	(17)	Tavan et al. (2019)
Dimensionless numbers	–	$Re=\frac{d_p v_s \rho}{\mu}; \quad Sc=\frac{\mu}{\rho D_m}; \quad Pe=\frac{Z v_s}{D_z}$	(18)	(Perry and Green, 2008; Soriano et al., 2016)

Table 3
Properties of fixed-bed and SMX solution.

Parameter		Symbol	Value	Unit
Equilibrium data	Maximum adsorption capacity	q_{max}	1.52	mg/g
	Energy constant	k_L	0.02	L/mg
	Adsorption capacity at equilibrium	q_0	0.155	mg/g
Fixed-bed	Bulk density	ρ_b	70.2	kg/m^3
	Bed diameter	D	0.022	m
	Bed porosity	ϵ_b	0.63	–
Sugarcane bagasse	SB particle porosity	ϵ_p	0.21	–
	SB particle density	ρ_b	1088.4	kg/m^3
	Average particle diameter	d_p	5.9×10^{-4}	m
	Specific surface area	S	2.55	m^2/g
SMX solution	Molar volume of SMX	V_m	173.1	cm^3/mol
	Density solution	P	998.6	kg/m^3
	Solvent association parameter	α_A	2.6	–
	Dynamic viscosity solution	μ	0.001	kg/m.s

breakthrough curves were obtained under conditions of flow rates of 2, 5, and 7 mL/min, and bed heights of 15 and 25 cm. Finally, the breakthrough time ($t_b \rightarrow C/C_0 = 0.05$), saturation time ($t_s \rightarrow C/C_0 = 0.75$), the adsorption capacity q_e (mg/g), and the fraction of the saturated bed was estimated H_b (%).

$$q_e = \frac{Q}{1000\ m} \int_{t=0}^{t=ts} C_R dt \tag{19}$$

$$H_b = \frac{Zt_b/t_s}{Z} * 100 \tag{20}$$

4. Results and discussion

The SMX adsorption onto sugarcane bagasse was carried at three flow rates (2, 5, and 7 mL/min) and two values of bed height (15 and 25 cm). Fig. 2a, b, and 2c show the experimental breakthrough curves at bed height of 15 cm and flow rates of 2, 5, and 7 mL/min, respectively. Whereas Fig. 2d, e, and 2f show the experimental breakthrough curves at bed height of 25 cm and flow rates of 2, 5, and 7 mL/min, respectively. The breakthrough and saturation times increase as the flow rate decreases (Table 4), hence the breakthrough and saturation times are greater at lower flow rates, it is because the interstitial velocity increases and the residence time of the SMX solution decreases as the flow rate increases (Babu and Gupta, 2005). Similarly, an increase in bed height significantly prolongs the breakthrough and saturation time of the column because there is a greater amount of adsorbent material available for SMX removal (Juela, 2020). Besides, the experimental adsorption capacity (q_e) decreased with flow rate, but no particular trend was observed with the change of bed height. The maximum adsorption capacity was obtained under conditions of a flow rate of 2 mL/min and a bed height of 25 cm; similarly, at the same

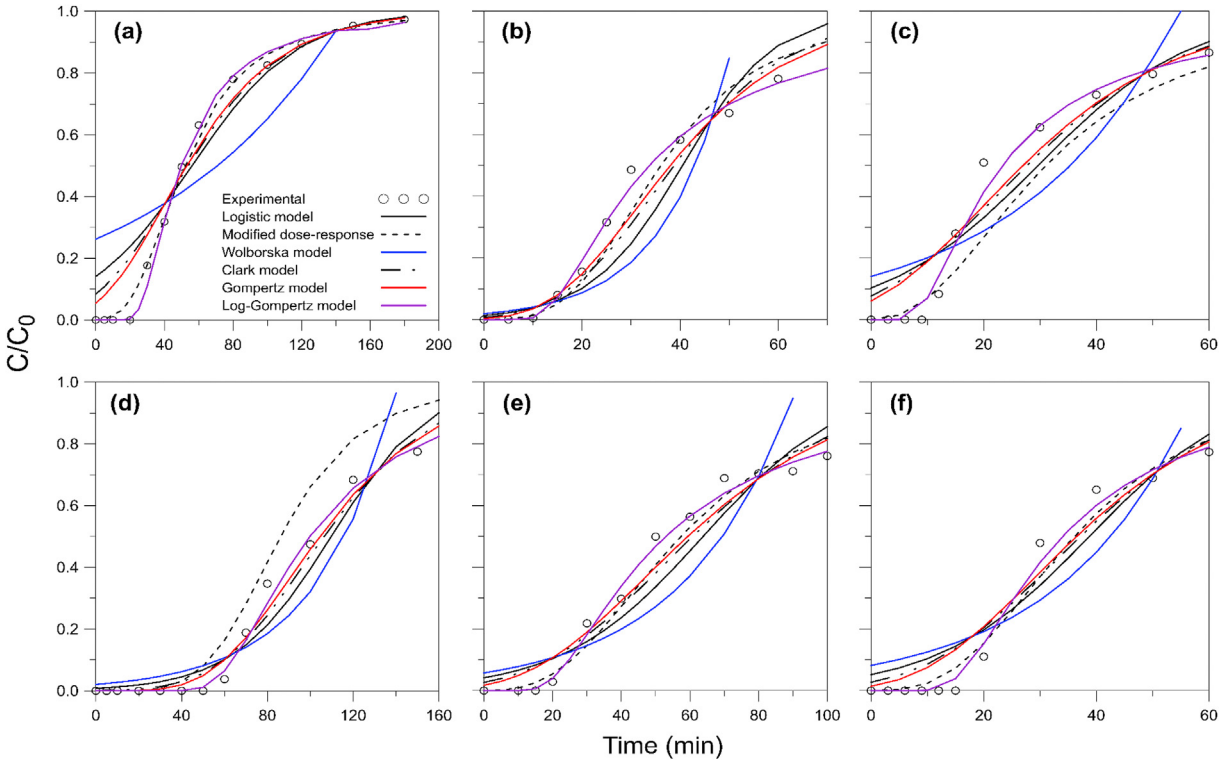

Fig. 2. Experimental and predicted breakthrough curves at flow rates of 2, 5, and 7 mL/min, 15 cm (a, b, c) and 25 cm (d, e, f) of bed height.

Table 4
Kinetic parameters of the seven analytical models.

Experimental	Q (mL/min) Z (cm)	2 15	5 15	7 15	2 25	5 25	7 25
	q_e (mg/g)	0.203	0.188	0.163	0.231	0.172	0.132
	t_b (min)	22.83	13.02	10.81	60.82	21.14	17.27
	t_s (min)	75.96	57.24	43.03	141.82	97.79	57.25
	H_b (%)	30.06	22.73	25.13	42.88	21.6	30.16
Logistic model	b	0.03	0.11	0.07	0.04	0.05	0.07
	a	1.81	4.32	2.17	4.82	3.14	2.91
	R^2	0.95	0.77	0.83	0.84	0.80	0.82
Yoon-Nelson model	k_{YN} (1/min)	0.03	0.11	0.07	0.04	0.05	0.07
	τ (min)	56.08	40.51	29.64	109.78	63.85	38.76
Bohart-Adams model	k_{BA} (L/mg min)	0.006	0.021	0.014	0.008	0.009	0.014
	N_0 (mg/L)	10.26	18.29	18.49	12.18	17.22	14.51
Thomas model	k_{Th} (L/mg min)	0.006	0.021	0.014	0.008	0.009	0.014
	q_F (mg/g)	0.146	0.261	0.264	0.181	0.256	0.215
Wolborska model	β (1/min)	0.05	0.35	0.24	0.08	0.15	0.18
	q_F (mg/g)	0.154	0.135	0.195	0.089	0.142	0.126
	R^2	0.65	0.63	0.62	0.68	0.66	0.70
Modified dose-response model	α'	2.78	3.35	2.30	4.50	2.72	2.90
	q_F (mg/g)	0.14	0.23	0.28	0.14	0.23	0.20
	R^2	0.99	0.93	0.93	0.91	0.94	0.92
Clark model	r (1/min)	0.028	0.067	0.057	0.031	0.034	0.056
	B	0.90	2.68	0.96	5.20	1.57	1.56
	R^2	0.98	0.89	0.89	0.91	0.88	0.87
Gompertz model	β_G (1/min)	0.027	0.056	0.052	0.027	0.029	0.049
	α_G	1.07	1.77	1.03	2.46	1.40	1.45
	R^2	0.98	0.93	0.92	0.94	0.91	0.89
Log-Gompertz model	β_G (1/min)	2.29	1.66	1.60	2.71	1.58	1.89
	α_G	8.57	5.49	4.65	12.09	5.92	6.30
	R^2	0.98	0.99	0.97	0.98	0.98	0.96

conditions, the highest fraction of the saturated bed was obtained. Besides, H_b increased with bed height in most cases, but no clear effect was observed with the change of flow rate. Considering these parameters, the optimal operative conditions, where the best performance of the sugarcane bagasse to remove SMX is achieved, were 2 mL/min of flow rate and 25 cm of bed height.

4.1. Fit with analytical models

The six experimental tests were fitted to seven analytical models; the predicted breakthrough curves by the models are shown in Fig. 2. The correlation coefficient (R^2) and the kinetic parameters of each model are shown in Table 4. As can be seen, high correlation coefficients $R^2 > 0.90$ were obtained with the Log-Gompertz and Modified dose-response models for all the adsorption tests, being the Log-Gompertz model the one that best reproduced the experimental data. The Clark and Gompertz models had also a good fit with the experimental data, their R^2 values are between 0.87 and 0.98. For the Logistic model, which groups the Yoon Nelson, Thomas, and Bohart-Adam models, R^2 values were obtained in the range of 0.77−0.95, while the worst fit was obtained with the Wolborska model with $R^2 < 0.69$. In other words, the R^2 values obtained with kinetic models which provide asymmetric breakthrough curves (the Log-Gompertz and Modified dose-response, Clark, and Gompertz models) were higher than the models wich represents symmetric sigmoidal curves (the Yoon Nelson, Thomas, and Bohart-Adam models) (Hu et al., 2020).

In Fig. 2, the predicted breakthrough curves by the Modified dose-response model were very close to the experimental curve. This model also had a good fit in the SMX adsorption with other adsorbents (Jaria et al., 2019). At conditions of 2 mL/min of flow rate and 15 cm of bed height, this model provides a high fit with the experimental curve, especially in the transitory and saturation zone; when the conditions change, the breakthrough curves of this model only coincide with the experimental data in the initial region, and for this reason, the correlation coefficient values are lower. The breakthrough curves predicted by the Clark and Gompertz models were very similar for all experimental tests. According to Hu et al. (2020) the Clark model will generate asymmetric breakthrough curves when the parameter $n \neq 2$; in this study, $n = 1.2$ (Zeas Solórzano and Zhunio Campoverde, 2019) indicates that the breakthrough curves are asymmetric and therefore have an acceptable fit with the experimental data. While the Wolborska model had not a good agreement with the experimental data in any region. Generally, this model is suitable to reproduce the initial region of the breakthrough curve ($C/C_0 < 0.5$), but in this case, its adjustment was low even in this region; this means that the SMX adsorption is not controlled by film diffusion (Das et al., 2020).

Of all analytical models analyzed in this study, the Log-Gompertz model was the one that best reproduced the experimental data; the predicted breakthrough curves coincide with the experimental data in most of the trajectory, but it was more accurate in the initial region of the curve where the rest of models failed. This model recently adopted for adsorption processes has also shown a good correlation with the breakthrough data in the adsorption of metals and dyes (Chu, 2020b). Chu (2020b) also proved that this model is better than the Logistic (the Thomas, Bohart-Adams, and Yoon-Nelson models) and Gompertz models, and this research work shows that this model can even have a better fit than the popular Modified dose-response model. The main justification for these results is that the Log-Gompertz model was developed to fit asymmetric breakthrough curves, such as those obtained in this study, whereas the Bohart-Adams, Thomas, and Yoon-Nelson models only predict symmetric sigmoidal curves, which is a great drawback for adsorption studies with asymmetric data (Darweesh and Ahmed, 2017; Reynel-Avila et al., 2015).

Although the equations of the Gompertz and modified dose-response models also are essentially asymmetric, their fit is not enough especially in the initial and final region of the breakthrough curve; this happens when the experimental curve exhibits a pronounced degree of tailing (Chu, 2020b). On the other hand, the Log-Gompertz model, which is a modified version of the Gompertz model, is able to effectively model a strong asymmetry because it transforms the independent variable t (from the Gompertz model) to the term ln (t), which improves the fit with the breakthrough data in the initial and final region.

A drawback of the Log-Gompertz and Gompertz models is that their parameters do not provide valuable information regarding the adsorption process; that is because there is not a mechanistic undertone behind these models. The equation of the Gompertz model equation was initially developed to explain the human mortality curve, and therefore, it is not based on any assumptions regarding adsorption mechanisms (Gompertz, 1825). Accordingly, its parameters do not elucidate useful information on the dominant mechanisms in the adsorption of SMX onto SB. However, it was observed that these parameters change as the operating conditions of the fixed-bed column change; Both β_G and α_G of the Log-Gompertz model decrease with increasing flow rate, but increasing with bed height. Although the same parameters with the Gompertz model did not show a clear trend with changes in flow rate and bed height.

In most cases, the kinetic constant of the Bohart-Adams and Thomas models increased with flow rate, hence the bed saturation is rapid at high flow rates (Jaria et al., 2019). Similarly, the time in which SMX in the effluent reaches 50% of the initial concentration (τ), in the Yoon-Nelson model, decreases with the increase in the flow rate but increases with the increase in the bed height. This is logical as the experimental breakthrough curves shift to the right with decreasing flow rate and increasing bed depth. A similar effect was observed in the adsorption of tetracycline with active carbon (Marzbali and Esmaieli, 2017).

Both Modified dose-response and Thomas models assume no axial dispersion, external and internal diffusion resistances extremely small, and the second-order reversible reaction kinetics. Although both of these models are based on the same assumptions, their adjustment to the experimental data is different; this is due to the modified dose-response model was proposed to minimize the mathematical errors of the Thomas model equation, for this reason, this model gives a better adjustment to the experimental data (Yan et al., 2001). Despite the best fitting of the Modified dose-response model, the adsorption capacity determined by this model in some cases is higher and in other cases is lower than experimentally ones (Table 4). Besides, a decrease of q_F values of the Modified dose-response model when increasing the flow rate was expected, just as it happened in experimentation, but it was not observed. The same happened with the adsorption capacity predicted by the Thomas and Wolborska models; this behavior has been also observed in other studies (Dorado et al., 2014; Jaria et al., 2019). Regarding the amount of adsorbate retained per bed volume (N_0) of the Bohart-Adams model, it also should decrease as the flow rate increases, but it had a similar effect to q_F in the Thomas and Modified dose-response models. In all cases, no direct effect on q_F and N_0 was observed with bed height. Similar to other models, the parameters r and B of the Clark model have no clear relationship with the change of flow rate and bed height.

4.2. Comparison of the best analytical model with the mechanistic model

The dynamic behavior of the SMX in the column packed with SB was also studied with a theoretical mechanistic model, which is based on the film and intraparticle diffusions, and on the axial dispersion phenomenon. This mechanistic model was compared with the best-fit analytical model (Log-Gompertz model), and the sum squared errors (SSE) and the correlation coefficient (R^2) were used as error functions to analyze the fit between experimental and predicted breakthrough curves. The experimental and predicted breakthrough curves by the Log-Gompertz and mechanistic models are shown in Fig. 3, while the values of SSE and R^2 for both models are shown in Table 5.

$$SSE = \sum_{i=1}^{n} \left(x_{i,cal} - x_{i,meas}\right)^2 \tag{21}$$

$$R^2 = 1 - \frac{\sum_{i=1}^{n} \left(x_{i,cal} - x_{i,meas}\right)^2}{\sum_{i=1}^{n} \left(x_{i,meas} - \bar{x}\right)^2} \tag{22}$$

The C/C_0 values predicted by the theoretical model agree well with the experimental data, as good as the Log-Gompertz model. However, the predicted curves with the analytical model are more consistent, especially in the initial and final region of the

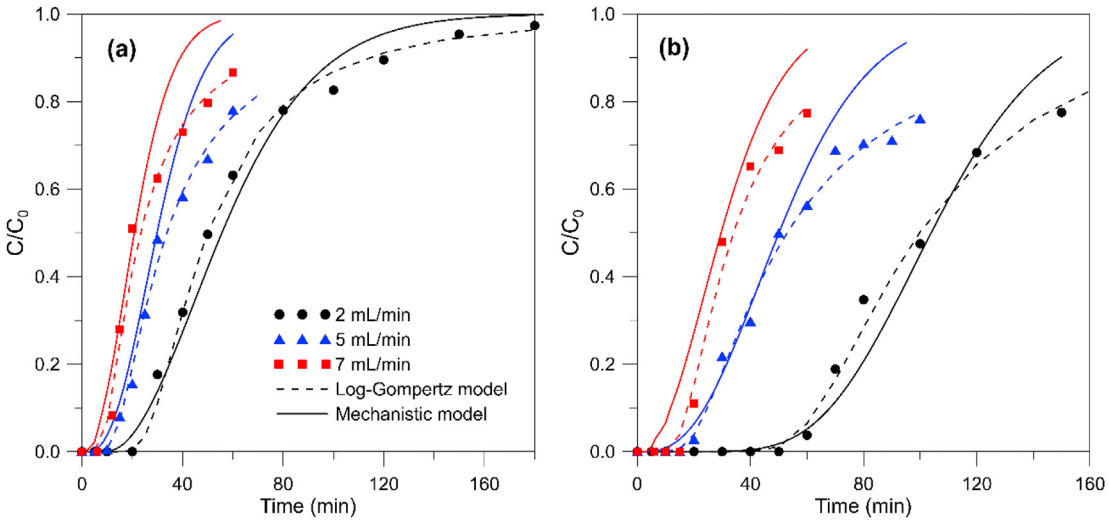

Fig. 3. Experimental and predicted breakthrough curves by the Log-Gompertz and mechanistic models at 15 cm (a) and 25 cm (b) of bed height.

Table 5
Error functions for Log-Gompertz and mechanistic models.

Test	Q (mL/min)	Z (cm)	Log-Gompertz model		Mechanistic model	
			SSE	R^2	SSE	R^2
1	2	15	0.007	0.996	0.026	0.987
2	5	15	0.006	0.993	0.127	0.887
3	7	15	0.016	0.987	0.099	0.922
4	2	25	0.007	0.992	0.043	0.957
5	5	25	0.008	0.993	0.118	0.892
6	7	25	0.011	0.989	0.113	0.895

breakthrough curve; whereas the mechanistic model does not accurately correlate with experimental data in the final region of the curve. While in the transitional stage both models show a good fit. The breakthrough and saturation times of simulated curves with the theoretical model are less than the experimental ones, which theoretically represents a fast adsorption rate of SMX. Conversely, these operating times were very similar to the curves predicted by the analytical model. The R^2 and SSE values are given in Table 5. The predicted breakthrough curve by the Log-Gompertz model has higher R^2 values ($R^2 > 0.98$) and lower SSE values (SSE<0.016) than the mechanistic model in all tests; this confirms that the analytical model fits better with experimental breakthrough data. Even though the R^2 and SSE values were lower than the analytical model, the theoretical model proposed for the SMX adsorption onto SB predicts the breakthrough curves with acceptable precision; correlation coefficients higher than 0.87 and SSE values lower than 0.13 were obtained, and according to the values of these statistical indicators, predicted results are not highly consistent with experimental data (William Kajjumba et al., 2019). A noticeable deviation between breakthrough data and the mechanistic breakthrough curve was obtained in the final region. The main reason may be the tail behavior of the experimental breakthrough curves; this phenomenon has been observed in other mechanistic models where the simulated curve does not converge with the final region of the experimental data (Chu, 2020b; Izquierdo et al., 2010; Vera et al., 2021). Many authors suggest that the factors responsible for the tailing behavior should be included in the mechanistic model to get better breakthrough curves (Chu, 2020b). Although the mechanistic model does not provide great precision in the final region, it showed a good correlation in the initial and transition stage of the curves, which could be useful because in the practice the adsorbent is replaced in the breakthrough time. Correlation coefficients higher than 0.92, and sum squared errors less than 0.06 were obtained up to C/C_0 of 0.6.

Although the breakthrough curves predicted by the Log-Gumpertz model had a good correlation with the experimental ones, the good similarity between the results of the mechanistic model and the experimental results is encouraging and supports the precision of the assumptions made, empirical correlations used, and model parameters calculated. Furthermore, when comparing both models, it should be considered that the mechanistic model is a theoretical model that for its application only requires basic information, i.e. adsorbent and adsorbate properties, and operating conditions. Hence, a breakthrough curve can be simulated without prior experimentation. Whereas the analytical model requires breakthrough data, that is, it is necessarily necessary to carry out experimental adsorption studies before its application. Hence, this model is only a simple tool for experimental data fitting, without providing useful information regarding the main mechanisms involved in the adsorption process. Furthermore, as we discussed previously, their parameters do not show a clear relationship with the change in operating conditions, and these in certain cases have different behavior from those observed in experimentation; hence their practical usefulness is questionable. Undoubtedly, to understand better the complex mechanisms of adsorption, it is necessary to develop more rigorous mechanics models. The mechanistic model proposed in this study was validated with lab-scale column experiments and showed a good agreement with the experimental data; therefore, the same model can be used with confidence to predict the breakthrough curves for the same adsorbent/adsorbate system on large scale columns, such as pilot or industrial adsorption columns. In this way, it would be possible to estimate breakthrough and saturations times on these columns and compare them with conventional activated carbon columns. For these reasons, for the purposes of design, scaling, and optimization of adsorption columns the mechanistic models have shown to be more useful (Burkert et al., 2011; Unuabonah et al., 2019).

4.3. Mechanistic model parameters and the relative importance of axial dispersion

In Fig. 3a and b, the breakthrough curves were simulated with values of global mass transfer coefficient (K_i) and axial dispersion coefficient (D_z) determined using the empirical correlations presented in the Eqs. (10) and (11), without using the experimental data shown. Both K_i and D_z vary with feed flow rate but remain invariant with bed height as shown in Fig. 4a and Table 6. The justification for this is because the K_i and D_z values are estimated by

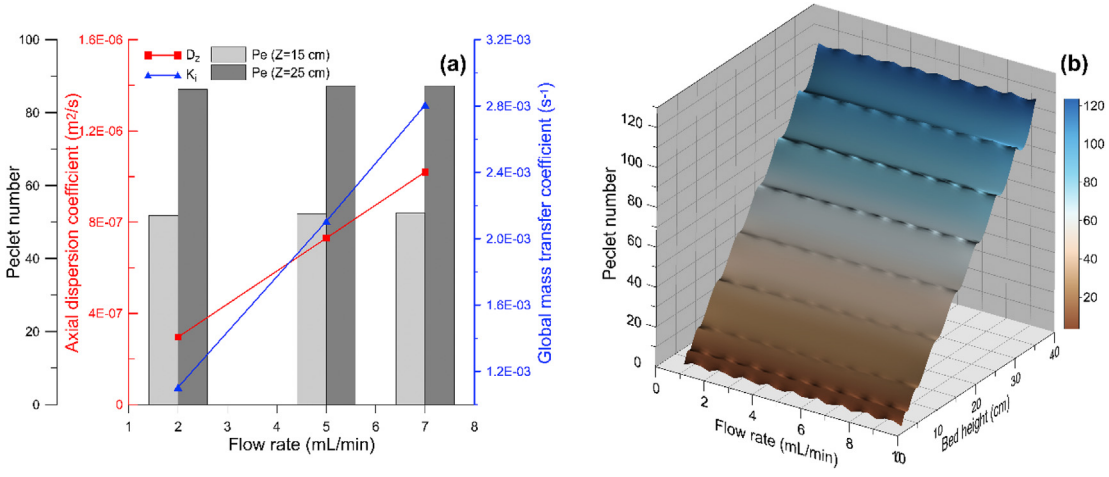

Fig. 4. Variation of the global mass transfer and axial dispersion coefficients (a), and the Peclet number (b) with flow rate and bed height.

Table 6
Film diffusion and intraparticle diffusion parameters.

Q (mL/min)	H (cm)	k_f x10^{-6} (m/s)	D_s x10^{-12} (m^2/s)	D_p x10^{-12} (m^2/s)	D_{ep} x10^{-12} (m^2/s)	K_i x10^{-3} (1/s)	D_z x10^{-7} (m^2/s)	γ_p	γ_f
2	15	6.61	3.86	9.89	6.68	1.10	2.96	0.26	0.15
5	15	8.46	3.86	9.89	6.68	2.11	7.30	0.66	0.29
7	15	9.33	3.86	9.89	6.68	2.81	10.2	0.92	0.38

empirical correlations that only consider the hydrodynamic conditions, depending mainly on the fluid velocity for any adsorbate-adsorbent system (Lin et al., 2017; Saadi et al., 2019). The parameter K_i combined both the film diffusion and intraparticle diffusion; the film diffusion coefficient lowered with increasing flow rates indicating that the external mass transfer resistance is less influential (Quek and Al-Duri, 2007). On the other hand, the surface diffusion and pore diffusion coefficients remained constant for the variation in flow rate and bed height (Table 6). The Peclet number (*Pe*) was also affected by the change in flow rate and bed height (Fig. 4a and b), *Pe* increases proportionally with both flow rate and bed height, although the change was more significant with the bed height (from 51.8 to 86.3 when it goes from 15 to 25 cm) than the flow rate (from 51.8 to 52.44 when it goes from 2 to 7 mL/min); this happens because the Peclet number is based on the length of the fixed-bed (Eq. (18)).

Additionally, the relative importance of axial dispersion was assessed by comparison with the other rate mechanisms (i.e. intraparticle diffusion and external film mass transfer); the parameters γ_p and γ_f were used, represented in Eq. (23) and showed in Table 6 (Cooney, 1991).

$$\gamma_p = \left[\frac{\alpha^2(1-\varepsilon_b)}{15\varepsilon_b}\right]\left(\frac{r_p^2 K}{D_{ep} D_z}\right)$$
$$\gamma_f = \left[\frac{\alpha^2(1-\varepsilon_b)}{3\varepsilon_b}\right]\left(\frac{r_p K^2}{k_f D_z}\right) \quad (23)$$

where K is the distribution ratio equal to q_0/C_0, α is the velocity of constant pattern front, and it was estimated with the correlation of Cooney (1991). As Cooney (1991) has shown, when γ values are higher than 1, axial dispersion can safely be ignored. However, for this study, the parameters γ_p and γ_f were lower than 1 for all studies; so, in this case, the axial dispersion would be significant. The axial dispersion phenomenon usually is neglected for liquid-phase systems, but many studies have shown that when the particle sizes and/or the flow rates are much smaller than usual, the parameters γ_p and γ_f could very easily be on the order of 1 or less, in which case axial dispersion would be significant as it happens in this study (Davila-Guzman et al., 2016; Díaz-Blancas et al., 2020; Franco et al., 2020; Saadi et al., 2015). Additionally, in all tests $\gamma_f < \gamma_p$, which means that the interparticle diffusion is more relevant than film diffusion, and the difference between γ_p and γ_f is higher as flow rate increases (Cooney, 1991).

Finally, a sensitivity analysis was developed in order to evaluate the relative importance of the global mass transfer coefficient and axial dispersion coefficient in the prediction of the breakthrough curves. The effect of K_i on the breakthrough curves was studied by varying K_i from its base value (0.0011 s^{-1}, estimated for the simulated breakthrough curves at 2 mL/min), while the value of the axial dispersion coefficient remained constant at 2.96×10^{-7} m^2/s. Three K_i values were used, which were calculated using Eq. (10). The influence of K_i on the breakthrough curves is shown in Fig. 5a. A similar analysis was performed for D_z. Three D_z values were studied, starting from its base value (2.96×10^{-7} m^2/s, used in the simulated curves at 2 mL/min) while the K_i value was kept constant at 0.0011 s^{-1}. Fig. 5b shows the results obtained.

The variation of K_i from 0.0011 to 0.011 s^{-1} produces an increase in the breakthrough times and a decrease in the saturation times; this is mainly due to the increase in the slope of the breakthrough curve as K_i increases. According to the LDF kinetic model, the adsorption rate of SMX is directly proportional to the mass transfer coefficient, hence high K_i values increase the adsorption rate; increasing K_i also means that the external film resistance, and diffusion and intraparticle resistances decrease; so the saturation rate increases rapidly (Xu et al., 2013). Something that is also

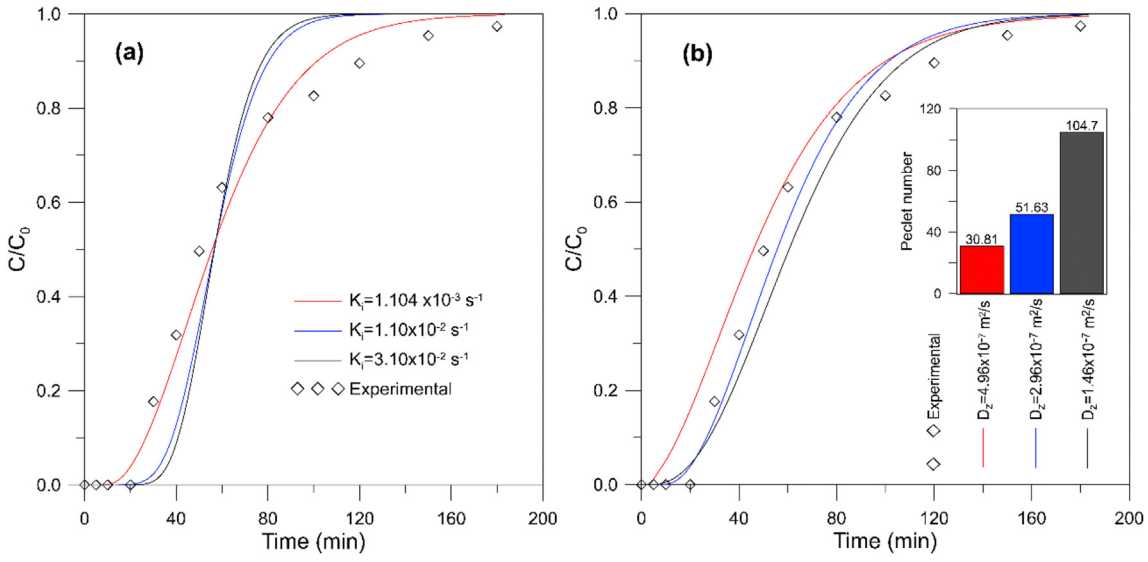

Fig. 5. Effect of global mass transfer coefficient (a) and axial dispersion coefficient (b) on the predicted breakthrough curves.

evident is that the rise in K_i causes the curves to start to converge after a certain value. In Fig. 5a, the curve of $K_i = 0.011\ s^{-1}$ is very close and practically coincident to the curve of $K_i = 0.031\ s^{-1}$, despite the notable difference in the values of the global mass transfer coefficient. Which could mean that for higher values of K_i the curves will overlap, and the variation in the SMX adsorption rate would become smaller and smaller. As a result, for a higher value of K_i, the adsorption rate could be roughly constant. Similar results were obtained in other fixed-bed column adsorption simulations (Aguilera and Gutiérrez Ortiz, 2016; Shekhar, 2014).

The axial dispersion coefficient groups the effects of turbulence, flow division, and reincorporation around particles, Taylor dispersion, channeling, and wall effects suffered by the fluid when circulating through the porous bed (Lin et al., 2017). In Fig. 5b, the increase in D_z from 1.46×10^{-7} to $4.96 \times 10^{-7}\ m^2/s$ causes the breakthrough and saturation times to shift to the left, causing saturation of the bed in a shorter time and lower adsorption capacities. This behavior of the breakthrough curve is reasonable since at high values of D_z the effects of axial mixing will be considerable, reducing the efficiency in the adsorption process and producing a rapid saturation of the bed (Aguilera and Gutiérrez Ortiz, 2016). Another important effect on the variation of D_z is reflected in *Pe*. From Fig. 5b, it is observed that when D_z decreases from 4.96×10^{-7} to $1.46 \times 10^{-7}\ m^2/s$, *Pe* increases from 30.81 to 104.7. Furthermore, with D_z values less than $1.46 \times 10^{-7}\ m^2/s$, *Pe* will be sufficiently greater than 100 and the axial dispersion phenomenon will not have any influence on the breakthrough curves. If the axial dispersion were neglected in the simulation ($D_z = 0\ m^2/s$), the breakthrough curve obtained would be very similar to that obtained with $D_z = 1.46 \times 10^{-7}\ m^2/s$, and it would differ significantly from the simulated curve with axial dispersion ($D_z = 2.96 \times 10^{-7}\ m^2/s$). Therefore, it can be inferred againthat the axial dispersion phenomenon is significant in the SMX adsorption with SB. This may be the main reason why the breakthrough curves predicted by analytical models are not accurate and differ from the experimental data, since most of these models do not take this phenomenon into account (Unuabonah et al., 2019; Xu et al., 2013).

5. Conclusions

Experimental breakthrough curves at different flow rates and bed heights were used to fit the classical analytical models. The Modified dose-response and Log-Gompertz models were the two best that showed good capabilities for breakthrough data fitting. However, their kinetic parameters did not provide relevant information about the adsorption process of SMX on SB, and in certain cases, these parameters had a different behavior from that observed in the experimentation. The Log-Gompertz model, which was the one that best reproduced the experimental asymmetric breakthrough curves, was compared with a mechanistic model that accounts for external and intraparticle diffusion, and axial dispersion. Both models showed good agreement with experimental data, being the Log-Gompertz model that showed a slightly better fit. Useful parameters such as the global mass transfer coefficient, axial dispersion coefficient, pore diffusion coefficient, and surface diffusion coefficient were estimated with the mechanistic model. Finally, the model showed the importance of the axial dispersion in the SMX adsorption on a lab scale. This model can be used with confidence for purposes of design, scaling, and optimization of adsorption columns.

Credit author statement

Diego Juela: Investigation, Formal analysis, Writing – original draft, Writing – review & editing. Mayra Vera: Methodology, Writing – original draft, Conceptualization. Christian Cruzat: Investigation, Formal analysis. Ximena Alvarez: Investigation. Eulalia Vanegas: Conceptualization, Writing – review & editing, Supervision, Validation, Resources, Funding acquisition, Project administration.

Declaration of competing interest

The authors declare that they have no known competing financial interests or personal relationships that could have appeared to influence the work reported in this paper.

Acknowledgements

The authors would like to acknowledge to Secretaría Nacional de Educación Superior, Ciencia, Tecnología e Innovación (SENESCYT) and Dirección de Investigación de la Universidad de Cuenca (DIUC) for financing through the project PIC-18-INE-UC-001 (INEDITA).

References

Aguilera, P.G., Gutiérrez Ortiz, F.J., 2016. Prediction of fixed-bed breakthrough curves for H2S adsorption from biogas: importance of axial dispersion for design. Chem. Eng. J. 289, 93–98. https://doi.org/10.1016/j.cej.2015.12.075.

Ahmad, S., Wong, Y.C., Veloo, K.V., 2018. Sugarcane bagasse powder as biosorbent for reactive red 120 removals from aqueous solution. IOP Conf. Ser. Earth Environ. Sci. 140, 012027 https://doi.org/10.1088/1755-1315/140/1/012027.

Ahmed, M.J., Hameed, B.H., 2018. Removal of emerging pharmaceutical contaminants by adsorption in a fixed-bed column: a review. Ecotoxicol. Environ. Saf. 149, 257–266. https://doi.org/10.1016/j.ecoenv.2017.12.012.

Babu, B.V., Gupta, S., 2005. Modeling and simulation of fixed bed adsorption column: effect of velocity variation. i-manager's. J. Futur. Eng. Technol. 1, 60–66. https://doi.org/10.26634/jfet.1.1.966.

Bakka, A., Mamouni, R., Saffaj, N., Laknifli, A., Aziz, K., Roudani, A., 2020. Removal of bifenthrin pesticide from aqueous solutions by treated patellidae shells using a new fixed bed column filtration technique. Process Saf. Environ. Protect. 143, 55–65. https://doi.org/10.1016/j.psep.2020.06.030.

Burkert, C.A.V., Barbosa, G.N.O., Mazutti, M.A., Maugeri, F., 2011. Mathematical modeling and experimental breakthrough curves of cephalosporin C adsorption in a fixed-bed column. Process Biochem. 46, 1270–1277. https://doi.org/10.1016/j.procbio.2011.02.016.

Chen, B., Sun, W., Wang, C., Guo, X., 2017. Size-dependent impact of inorganic nanoparticles on sulfamethoxazole adsorption by carbon nanotubes. Chem. Eng. J. 316, 160–170. https://doi.org/10.1016/j.cej.2017.01.087.

Chu, K.H., 2020a. Breakthrough curve analysis by simplistic models of fixed bed adsorption: in defense of the century-old Bohart-Adams model. Chem. Eng. J. 380, 122513 https://doi.org/10.1016/j.cej.2019.122513.

Chu, K.H., 2020b. Fitting the Gompertz equation to asymmetric breakthrough curves. J. Environ. Chem. Eng. 8, 103713 https://doi.org/10.1016/j.jece.2020.103713.

Cooney, D.O., 1991. The importance OF axial dispersion IN liquid-phase fixed-bed adsorption operations. Chem. Eng. Commun. 110, 217–231. https://doi.org/10.1080/00986449108939951.

da Silva Rodrigues, D.A., da Cunha, C.C.R.F., Freitas, M.G., de Barros, A.L.C., e Castro, P.B.N., Pereira, A.R., de Queiroz Silva, S., da Fonseca Santiago, A., de Cássia Franco Afonso, R.J., 2020. Biodegradation of sulfamethoxazole by microalgae-bacteria consortium in wastewater treatment plant effluents. Sci. Total Environ. 749, 141441 https://doi.org/10.1016/j.scitotenv.2020.141441.

Danckwerts, P.V., 1953. Continuous flow systems. Chem. Eng. Sci. 2, 1–13. https://doi.org/10.1016/0009-2509(53)80001-1.

Darweesh, T.M., Ahmed, M.J., 2017. Adsorption of ciprofloxacin and norfloxacin from aqueous solution onto granular activated carbon in fixed bed column. Ecotoxicol. Environ. Saf. 138, 139–145. https://doi.org/10.1016/j.ecoenv.2016.12.032.

Das, S., Barui, A., Adak, A., 2020. Montmorillonite impregnated electrospun cellulose acetate nanofiber sorptive membrane for ciprofloxacin removal from wastewater. J. Water Process Eng. 37, 101497 https://doi.org/10.1016/j.jwpe.2020.101497.

Davila-Guzman, N.E., Cerino-Córdova, F.J., Soto-Regalado, E., Loredo-Cancino, M., Loredo-Medrano, J.A., García-Reyes, R.B., 2016. A mass transfer model for the fixed-bed adsorption of ferulic acid onto a polymeric resin: axial dispersion and intraparticle diffusion. Environ. Technol. 37, 1914–1922. https://doi.org/10.1080/09593330.2015.1135993.

Díaz-Blancas, V., Aguilar-Madera, C.G., Flores-Cano, J.V., Leyva-Ramos, R., Padilla-Ortega, E., Ocampo-Pérez, R., 2020. Evaluation of mass transfer mechanisms involved during the adsorption of metronidazole on granular activated carbon in fixed bed column. J. Water Process Eng. 36, 101303 https://doi.org/10.1016/

j.jwpe.2020.101303.
Dima, J.B., Ferrari, M., Zaritzky, N., 2020. Mathematical modeling of fixed-bed columns adsorption: hexavalent chromium onto chitosan flakes. Ind. Eng. Chem. Res. 59, 15378–15386. https://doi.org/10.1021/acs.iecr.0c02004.
Dorado, A.D., Gamisans, X., Valderrama, C., Solé, M., Lao, C., 2014. Cr(III) removal from aqueous solutions: a straightforward model approaching of the adsorption in a fixed-bed column. J. Environ. Sci. Heal. Part A 49, 179–186. https://doi.org/10.1080/10934529.2013.838855.
Ekpeghere, K.I., Lee, J.-W., Kim, H.-Y., Shin, S.-K., Oh, J.-E., 2017. Determination and characterization of pharmaceuticals in sludge from municipal and livestock wastewater treatment plants. Chemosphere 168, 1211–1221. https://doi.org/10.1016/j.chemosphere.2016.10.077.
Franco, D.S.P., Fagundes, J.L.S., Georgin, J., Salau, N.P.G., Dotto, G.L., 2020. A mass transfer study considering intraparticle diffusion and axial dispersion for fixed-bed adsorption of crystal violet on pecan pericarp (Carya illinoensis). Chem. Eng. J. 397, 125423 https://doi.org/10.1016/j.cej.2020.125423.
Gompertz, B., 1825. On the nature of the function expressive of the law of human mortality, and on a new mode of determining the value of life contingencies. Phil. Trans. Roy. Soc. Lond. 115, 513–583. https://doi.org/10.1098/rstl.1825.0026.
Hu, Q., Xie, Y., Zhang, Z., 2020. Modification of breakthrough models in a continuous-flow fixed-bed column: mathematical characteristics of breakthrough curves and rate profiles. Separ. Purif. Technol. 238, 116399 https://doi.org/10.1016/j.seppur.2019.116399.
Izquierdo, M., Gabaldón, C., Marzal, P., Álvarez-Hornos, F.J., 2010. Modeling of copper fixed-bed biosorption from wastewater by Posidonia oceanica. Bioresour. Technol. 101, 510–517. https://doi.org/10.1016/j.biortech.2009.08.018.
Jaria, G., Calisto, V., Silva, C.P., Gil, M.V., Otero, M., Esteves, V.I., 2019. Fixed-bed performance of a waste-derived granular activated carbon for the removal of micropollutants from municipal wastewater. Sci. Total Environ. 683, 699–708. https://doi.org/10.1016/j.scitotenv.2019.05.198.
Johansson, C.H., Janmar, L., Backhaus, T., 2014. Toxicity of ciprofloxacin and sulfamethoxazole to marine periphytic algae and bacteria. Aquat. Toxicol. 156, 248–258. https://doi.org/10.1016/j.aquatox.2014.08.015.
Juela, D.M., 2020. Comparison of the adsorption capacity of acetaminophen on sugarcane bagasse and corn cob by dynamic simulation. Sustain. Environ. Res. 30, 23. https://doi.org/10.1186/s42834-020-00063-7.
Kavand, M., Fakoor, E., Mahzoon, S., Soleimani, M., 2018. An improved film–pore–surface diffusion model in the fixed-bed column adsorption for heavy metal ions: single and multi-component systems. Process Saf. Environ. Protect. 113, 330–342. https://doi.org/10.1016/j.psep.2017.11.009.
Klein, E.Y., Van Boeckel, T.P., Martinez, E.M., Pant, S., Gandra, S., Levin, S.A., Goossens, H., Laxminarayan, R., 2018. Global increase and geographic convergence in antibiotic consumption between 2000 and 2015. Proc. Natl. Acad. Sci. Unit. States Am. 115, E3463–E3470. https://doi.org/10.1073/pnas.1717295115.
Li, H., He, J., Chen, K., Shi, Z., Li, M., Guo, P., Wu, L., 2020. Dynamic adsorption of sulfamethoxazole from aqueous solution by lignite activated coke. Materials 13, 1785. https://doi.org/10.3390/ma13071785.
Lin, X., Huang, Q., Qi, G., Shi, S., Xiong, L., Huang, C., Chen, Xuefang, Li, H., Chen, Xinde, 2017. Estimation of fixed-bed column parameters and mathematical modeling of breakthrough behaviors for adsorption of levulinic acid from aqueous solution using SY-01 resin. Separ. Purif. Technol. 174, 222–231. https://doi.org/10.1016/j.seppur.2016.10.016.
Liu, X., Lu, S., Guo, W., Xi, B., Wang, W., 2018a. Antibiotics in the aquatic environments: a review of lakes, China. Sci. Total Environ. 627, 1195–1208. https://doi.org/10.1016/j.scitotenv.2018.01.271.
Liu, X., Lu, S., Meng, W., Zheng, B., 2018b. Residues and health risk assessment of typical antibiotics in aquatic products from the Dongting Lake, China—"Did you eat 'Antibiotics' today? Environ. Sci. Pollut. Res. 25, 3913–3921. https://doi.org/10.1007/s11356-017-0745-0.
Marzbali, M.H., Esmaieli, M., 2017. Fixed bed adsorption of tetracycline on a mesoporous activated carbon: experimental study and neuro-fuzzy modeling. J. Appl. Res. Technol. 15, 454–463. https://doi.org/10.1016/j.jart.2017.05.003.
Masri, A.K., Yen, T.W., Ahmad, M.A., Karim, S., 2020. Graphene-based nanomaterial for the removal of sulfamethoxazole in water. Mater. Today Proc. 31, 198–201. https://doi.org/10.1016/j.matpr.2020.02.236.
Naidu, H., Mathews, A.P., 2021. Linear driving force analysis of adsorption dynamics in stratified fixed-bed adsorbers. Separ. Purif. Technol. 257, 117955 https://doi.org/10.1016/j.seppur.2020.117955.
Nardy Ribeiro, A.V.F., Cruz Cosmo, P. da, Godoi Pereira, M. de, Dalfior, B.M., Gonçalves, G. dos S., Jennings Licinio, M.V.V., 2011. Use of sugarcane bagasse for adsorption of tetracycline in aqueous medium. Indian J. Appl. Res. 4, 10–14. https://doi.org/10.15373/2249555X/JAN2014/4.
Ohashi, H., Sugaware, T., Kikuchi, K., Konno, H., 1981. Correlation of liquid-side mass transfer coefficient for single particles and fixed beds. J. Chem. Eng. Jpn. 14, 433–438. https://doi.org/10.1252/jcej.14.433.
Peñafiel, M.E., Matesanz, J.M., Vanegas, E., Bermejo, D., Mosteo, R., Ormad, M.P., 2021. Comparative adsorption of ciprofloxacin on sugarcane bagasse from Ecuador and on commercial powdered activated carbon. Sci. Total Environ. 750, 141498 https://doi.org/10.1016/j.scitotenv.2020.141498.
Peñafiel, M.E., Matesanz, J.M., Vanegas, E., Bermejo, D., Ormad, M.P., 2020. Corncobs as a potentially low-cost biosorbent for sulfamethoxazole removal from aqueous solution. Separ. Sci. Technol. 55, 3060–3071. https://doi.org/10.1080/01496395.2019.1673414.
Perry, R.H., Green, D.W., 2008. Perry's Chemical Engineers' Handbook. New York: McGraw-Hill., New York.
Prasannamedha, G., Kumar, P.S., 2020. A review on contamination and removal of sulfamethoxazole from aqueous solution using cleaner techniques: present and future perspective. J. Clean. Prod. 250, 119553 https://doi.org/10.1016/j.jclepro.2019.119553.
Quek, S.Y., Al-Duri, B., 2007. Application of film-pore diffusion model for the adsorption of metal ions on coir in a fixed-bed column. Chem. Eng. Process. Process Intensif. 46, 477–485. https://doi.org/10.1016/j.cep.2006.06.019.
Reynel-Avila, H.E., Mendoza-Castillo, D.I., Bonilla-Petriciolet, A., Silvestre-Albero, J., 2015. Assessment of naproxen adsorption on bone char in aqueous solutions using batch and fixed-bed processes. J. Mol. Liq. 209, 187–195. https://doi.org/10.1016/j.molliq.2015.05.013.
Ruthven, D.M., 1984. Principles of Adsorption & Adsorption Processes. John Wiley & Sons, New York.
Saadi, R., Saadi, Z., Fazaeli, R., 2015. Determination of axial dispersion and overall mass transfer coefficients for Ni (II) adsorption on nanostructured γ-alumina in a fixed bed column: experimental and modeling studies. Desalin. Water Treat. 53, 2193–2203. https://doi.org/10.1080/19443994.2013.862869.
Saadi, Z., Fazaeli, R., Vafajoo, L., Naser, I., 2019. Adsorptive removal of apramycin antibiotic from aqueous solutions using Tween 80-and Triton X-100 modified clinoptilolite: experimental and fixed-bed modeling investigations. Int. J. Environ. Health Res. 1–26. https://doi.org/10.1080/09603123.2019.1612039.
Serna-Carrizales, C., Collins-Martínez, V.H., Flórez, E., Gomez-Duran, C.F.A., Palestino-Escobedo, A.G., Ocampo-Pérez, R., 2020. Adsorption of sulfamethoxazole, sulfadiazine and sulfametazine in single and ternary systems on activated carbon. Experimental and DFT computations. J. Mol. Liq. 114740 https://doi.org/10.1016/j.molliq.2020.114740.
Shekhar, S., 2014. Simulation of an Adsorption Column for the Removal of Ethyl Acetate from Air.
Soriano, A.N., Orfiana, O.N., Pangon, M.B.J., Nieva, A.D., Adornado, A.P., 2016. Simulated biosorption of Cd(II) and Cu(II) in single and binary metal systems by water hyacinth (Eichhornia crassipes) using aspen Adsorption®. ASEAN J. Chem. Eng. 16, 21–43.
Sun, Q., Li, M., Ma, C., Chen, X., Xie, X., Yu, C.-P., 2016. Seasonal and spatial variations of PPCP occurrence, removal and mass loading in three wastewater treatment plants located in different urbanization areas in Xiamen, China. Environ. Pollut. 208, 371–381. https://doi.org/10.1016/j.envpol.2015.10.003.
Tavan, Y., Hosseini, S.H., Ahmadi, G., Olazar, M., 2019. Mathematical model and energy analysis of ethane dehydration in two-layer packed-bed adsorption. Particuology 47, 33–40. https://doi.org/10.1016/j.partic.2018.11.001.
Tian, Y., Gao, B., Morales, V.L., Chen, H., Wang, Y., Li, H., 2013. Removal of sulfamethoxazole and sulfapyridine by carbon nanotubes in fixed-bed columns. Chemosphere 90, 2597–2605. https://doi.org/10.1016/j.chemosphere.2012.11.010.
Unuabonah, E.I., Omorogie, M.O., Oladoja, N.A., 2019. Modeling in adsorption: fundamentals and applications. In: Composite Nanoadsorbents. Elsevier, pp. 85–118. https://doi.org/10.1016/B978-0-12-814132-8.00005-8.
Välitalo, P., Kruglova, A., Mikola, A., Vahala, R., 2017. Toxicological impacts of antibiotics on aquatic micro-organisms: a mini-review. Int. J. Hyg Environ. Health 220, 558–569. https://doi.org/10.1016/j.ijheh.2017.02.003.
Vera, L., Bermejo, D., Uguña, M.F., Garcia, N., Flores, M., González, E., 2018. Fixed bed column modeling of lead(II) and cadmium(II) ions biosorption on sugarcane bagasse. Environ. Eng. Res. 24, 31–37. https://doi.org/10.4491/eer.2018.042.
Vera, L., Uguña, M.F., García, N., Flores, M., Vázquez, V., Aloma, I., 2016. Desarrollo de materielles sorbentes para la eliminación de metales pesados de las aguas residuales mineras [WWW Document]. Afinidad. URL. accessed 3.15.20. https://www.raco.cat/index.php/afinidad/article/view/312048.
Vera, M., Juela, D., Cruzat, C., Vanegas, E., 2021. Modeling and computational fluid dynamic simulation of acetaminophen adsorption using sugarcane bagasse. J. Environ. Chem. Eng., 105056 https://doi.org/10.1016/j.jece.2021.105056.
Wang, J., Wang, S., 2018. Microbial degradation of sulfamethoxazole in the environment. Appl. Microbiol. Biotechnol. 102, 3573–3582. https://doi.org/10.1007/s00253-018-8845-4.
Wilke, C.R., Chang, P., 1955. Correlation of diffusion coefficients in dilute solutions. AIChE J. 1, 264–270. https://doi.org/10.1002/aic.690010222.
Wilkinson, J., Hooda, P.S., Barker, J., Barton, S., Swinden, J., 2017. Occurrence, fate and transformation of emerging contaminants in water: an overarching review of the field. Environ. Pollut. 231, 954–970. https://doi.org/10.1016/j.envpol.2017.08.032.
William Kajjumba, G., Emik, S., Öngen, A., Kurtulus Özcan, H., Aydın, S., 2019. Modelling of adsorption kinetic processes—errors, theory and application. In: Advanced Sorption Process Applications. IntechOpen. https://doi.org/10.5772/intechopen.80495.
Wolborska, A., Pustelnik, P., 1996. A simplified method for determination of the break-through time of an adsorbent layer. Water Res. 30, 2643–2650. https://doi.org/10.1016/S0043-1354(96)00166-2.
Wu, M., Zhao, S., Tang, M., Jing, R., Shao, Y., Liu, X., Dong, Y., Li, M., Liao, Q., Lv, G., Zhang, Q., Meng, Z., Liu, A., 2019. Adsorption of sulfamethoxazole and tetracycline on montmorillonite in single and binary systems. Colloids Surfaces A Physicochem. Eng. Asp. 575, 264–270. https://doi.org/10.1016/j.colsurfa.2019.05.025.
Xu, Z., Cai, J.G., Pan, B.C., 2013. Mathematically modeling fixed-bed adsorption in aqueous systems. J. Zhejiang Univ. - Sci. 14, 155–176. https://doi.org/10.1631/jzus.A1300029.
Yan, G., Viraraghavan, T., Chen, M., 2001. A new model for heavy metal removal in a biosorption column. Adsorpt. Sci. Technol. 19, 25–43. https://doi.org/10.1260/

0263617011493953.
Yu, K., Ahmed, I., Won, D.-I., Lee, W.I., Ahn, W.-S., 2020. Highly efficient adsorptive removal of sulfamethoxazole from aqueous solutions by porphyrinic MOF-525 and MOF-545. Chemosphere 250, 126133. https://doi.org/10.1016/j.chemosphere.2020.126133.
Zeas Solórzano, S.J., Zhunio Campoverde, M.A., 2019. Determinación mediante técnica ultravioleta-visible de la capacidad de adsorción de mezclas de fármacos sobre residuos vegetales. University of Cuenca, Cuenca.
Zeng, S., Choi, Y.-K., Kan, E., 2021. Iron-activated bermudagrass-derived biochar for adsorption of aqueous sulfamethoxazole: effects of iron impregnation ratio on biochar properties, adsorption, and regeneration. Sci. Total Environ. 750, 141691 https://doi.org/10.1016/j.scitotenv.2020.141691.
Zhang, H., Du, M., Jiang, H., Zhang, D., Lin, L., Ye, H., Zhang, X., 2015. Occurrence, seasonal variation and removal efficiency of antibiotics and their metabolites in wastewater treatment plants, Jiulongjiang River Basin, South China. Environ. Sci. Process. Impacts 17, 225–234. https://doi.org/10.1039/C4EM00457D.